Science of the Total Environment 927 (2024) 171568

Contents lists available at ScienceDirect

Science of the Total Environment

journal homepage: www.elsevier.com/locate/scitotenv

Urban Flood Drifters (UFDs): Onset of movement

Daniel Valero [a,1], Arnau Bayón [b,*], Mário J. Franca [c]

[a] Department of Civil and Environmental Engineering, Imperial College London, United Kingdom
[b] Department of Hydraulic and Environmental Engineering, Universitat Politècnica de València, Spain
[c] Institute for Water and Environment, Karlsruhe Institute of Technology, Germany

HIGHLIGHTS

- We develop a mechanistic model to estimate stability curves of loose urban objects, which can be mobilized during extreme floods.
- We study the variability of the properties of UFDs and incorporate them into our stability analysis.
- We defne diferentiated mobility of UFDs and relate this to the flood hydrograph stage.
- We show that vans, caravans and RVs can be easier mobilized than lighter vehicles, with also larger associated flood hazards.
- Our study shows the potential for urban flood risk reduction through urban planning actions.

GRAPHICAL ABSTRACT

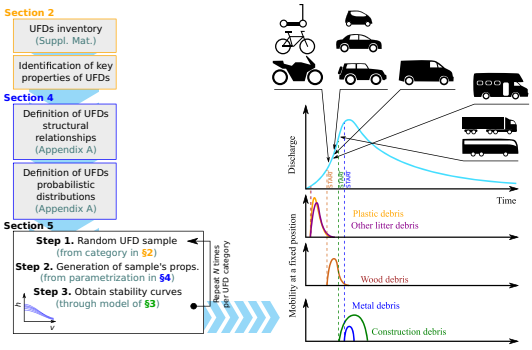

ARTICLE INFO

Editor: Fernando Pacheco

Keywords:
Flood
Plastic
Risk
UFD
Vehicles
Wood

ABSTRACT

Despite their catastrophic implications in flood events, the mobilization and transport of large, loose objects –termed Urban Flood Drifters (UFDs)– are often overlooked in flood management. These objects are inherent to anthropogenic activities, but are not designed to remain stable under flooding conditions, nor are usually considered in flood risk studies. This oversight stems from our limited understanding of how flowing water interacts with these heterogeneous objects. To bridge this knowledge gap, we introduce a mechanistic stability model that predicts the onset of UFD mobilization across a diverse array of loose objects, from plastics to heavy vehicles. We further enhance the reliability of our model by incorporating a Monte Carlo-based probabilistic framework that accounts for uncertainties and interdependencies among the input parameters. Our results show that plastic and other litter are the most mobile objects found in urban setups, being subject to incipient transport under frequent floods. These are followed by wood (anthropogenic or natural) and urban furniture. Vans, caravans and recreational vehicles (RVs) can be more mobile than other light-weight vehicles in low-gradient areas, whereas trucks and buses remain considerably more stable; although more hazardous, when mobilized. Construction and metal debris are predominantly stable in low-slope areas. When integrated with flood maps or two-dimensional (2D) hydrodynamic models, our stability curves can guide urban planning efforts to predict and mitigate the impacts of UFDs during extreme flood events.

* Corresponding author.
E-mail address: arbabar@upv.es (A. Bayón).
[1] Previously: Institute for Water and Environment, Karlsruhe Institute of Technology, Germany.

https://doi.org/10.1016/j.scitotenv.2024.171568
Received 24 November 2023; Received in revised form 4 March 2024; Accepted 6 March 2024
Available online 16 March 2024

1. Introduction

Floods exert significant impacts on human life, economic stability, environmental health, and cultural heritage (Hickey and Salas, 1995; Jonkman and Vrijling, 2008; Hammond et al., 2015; Arrighi, 2021). Between 2000 and 2019, floods affected 1.65 billion people globally, resulting in over 100,000 fatalities (Browder et al.; United Nations, 2023). Floods account for more than half of the total damage attributed to natural disasters since the 1980s (European Environment Agency, 2022). According to the World Economic Forum (2022), floods are one of the top three most frequent and severe weather events, predicted to displace over 200 million people by 2050 (Clement et al., 2021). Particularly in the European Union, approximately two-thirds of the aggregate damage caused by natural disasters since the 1980s can be attributed to hydrometeorological events (European Environment Agency, 2022). Moreover, a single flood event can yield direct costs running into thousands of millions of euros (European Environment Agency, 2022).

Low- and middle-income countries are acutely susceptible (Kahn, 2005), and even within countries with long tradition in flood defenses, a disparity exists in flood protection preparedness across urban areas of varying resources (Lindersson et al., 2023). Climate change, along with alterations in land use, exacerbate the situation by amplifying the frequency and intensity of floods (United Nations, 2020), thereby further exposing humans to these disastrous events (Winsemius et al., 2018).

A critical yet underexamined aspect of floods is their ability to mobilize Urban Flood Drifters (UFDs, Fig. 1), comprising loose objects commonly found in urban settings (Bayón et al., 2023). The definition of UFDs refers to objects that are essential to anthropogenic activities but, that under high enough flows, can become part of the flood and increase flood risk; see for instance the formation of a dike or the blocking of a bridge in Fig. 1A and B, respectively. The resultant hazards range from structural damage to buildings (Jalayer et al., 2018; Zhang et al., 2018) to the obstruction of critical flood relieving infrastructure (Kramer et al., 2015; Davidson et al., 2015) and disruption of roads therefore affecting emergency response (Pregnolato et al., 2017; Arrighi et al., 2019; Argyroudis et al., 2019). Despite growing awareness of the role of UFDs in floods (Dewals et al., 2021; Mohr et al., 2023; Ludwig et al., 2023), this phenomenon remains largely underrepresented in urban flood research and impact evaluations. Literature may have neglected this phenomenon since understanding its dynamics is exceptionally intricate and heavily reliant on case-specific scenarios. For selected UFDs, there are studies on their incipient motion. Existing research has largely concentrated on the stability of vehicles (Keller and Mitsch, 1992; Xia et al., 2014) and trash containers (Martínez-Gomariz et al., 2020), often under controlled, experimental conditions. As a consequence, several models can be found in literature, able to predict the mobilization of cars under flooding conditions (Arrighi et al., 2015; Martínez-Gomariz et al., 2018; Milanesi and Pilotti, 2020; Bocanegra et al., 2020; Shah et al., 2021), which have also been extended to trash containers (Martínez-Gomariz et al., 2020) and pedestrians stability (Martínez-Gomariz et al., 2016; Arrighi et al., 2017). Such mechanistic, laboratory scale studies, have only recently been extended to incipient motion of plastic debris (Waldschläger and Schüttrumpf, 2019; Goral et al., 2023; Mellink et al., 2023), and their transport (Valero et al., 2022; Lofty et al., 2023). However, a comprehensive hydro-mechanical framework to gauge the mobilization and transport of the wider range of UFDs is still lacking, thus limiting the precise forecasts of their impact in flood scenarios.

We observe that the mobilization flow conditions of UFDs can vary significantly while the physics describing their inception of movement are similar, provided that they are found loose. Our study aims to develop a robust mechanistic model capable of addressing a broader array of UFDs, as categorized in Table 1, and beyond the groups previously addressed in literature. By combining such a mechanistic model with a probabilistic approach that relies on readily accessible catalogue parameters, our model outlines the threshold conditions for flotation,

Fig. 1. Examples of UFDs categorized according to Table 1: A Sanliurfa, Turkey (credit: AFP, 2023), B Cedar Rapids, USA (credit: Roberson, 2008), and C Laishui, China (credit: Getty Images, 2012).

sliding, and toppling of various UFDs, considering simple flow variables (depth h and depth-averaged velocity v). We evaluate the performance of the model across different car types, based on prior studies on vehicular flood instability. Furthermore, we analyze the attributes' interdependencies among different UFDs, enabling a realistic mathematical profiling of these objects. By adopting a Monte Carlo technique, we account for uncertainties in estimating stability limit states, thereby capturing the inherent variability associated with the onset of mobilization of UFDs. The distribution of stability curves generated for each group of UFDs can be coupled with hydrodynamic modelling to better understand flood hazards.

2. Urban Flood Drifters and their key characteristics

Bayón et al. (2023) highlighted the diversity (Table 1) of UFDs in urban environments following catastrophic flooding, which can be grouped into two main categories: 1) typified UFDs, which correspond to standardized items found in catalogues and are manufactured with specific dimensions and weights, and 2) a heterogeneous mixture of diverse shapes and weights (UFD-H). For the first UFD category, two functional categories are discernible, namely vehicles (UFD-V) and furniture (UFD-F).

Bayón et al. (2023)'s statistical evaluation reveals a considerable prevalence of heterogeneous debris and drifters –including plastics, construction debris, wood–, furniture (both public and private), and even heavy vehicles. A review of this study and other investigations on urban flooding (Mignot et al., 2019; Smith et al., 2019a; O'Donnell and Thorne, 2020; Zevenbergen et al., 2020; Wing et al., 2022; Bates et al., 2023; Sanders et al., 2023) indicates that the stability characteristics of the majority of UFDs outlined in Table 1 remain largely unknown.

Table 1
Classification and grouping of UFDs based on the analysis of Bayón et al. (2023).

	Category	ID	Subcategory	Description
Typified UFDs	Vehicles (UFD-V)	V1	Two-wheelers	Bikes, motorbikes and e-scooters.
		V2	Cars	Cars and other light four-wheel vehicles designed to transport of passengers.
		V3	Vans	Vans and other heavy four-wheel vehicles designed to transport materials and stock.
		V4	Caravans & RVs	Vehicles designed to provide habitable space (RV: recreational vehicle).
		V5	Large heavy vehicles	Vehicles designed to transport a large amount of people or goods (buses, trucks, trains, boats, etc.).
	Furniture (UFD-F)	F1	Urban furniture	Facilities designed to provide a public service in streets (bins, waste containers, etc.).
		F2	Household furniture	Facilities from private front (and back) gardens that can be carried by floods (tanks, garden sheds, etc.).
Heterog. UFDs	(UFD-H)	DC	Construction	Debris that can be dragged from construction sites or damaged buildings.
		DM	Metal	Metal debris, predominantly of constructive origin (sheets, pipes, etc.).
		DP	Plastic	Plastics and textile objects of small dimensions and irregular shape.
		DW	Wood	Natural wood (trunks, branches, etc.) and processed wood.
		DO	Others	Other drifters of uncertain origin (food, tableware, leaves, sediment, etc.).

Earlier research frequently employed experimental setups, often involving scale models of cars, to analyze stability curves. These curves are derived from varying water depths and depth-averaged flow velocities under controlled hydraulic laboratory conditions (see, for example, Kramer et al., 2016; Smith et al., 2019b, for 1:1 scale models). Furthermore, theoretical models grounded in first principles have been developed and calibrated against experimental data to predict unstable conditions for specific car models (Xia et al., 2014; Shah et al., 2021) and trash bins (Martínez-Gomariz et al., 2020). Following Martínez-Gomariz et al. (2020) and Smith et al. (2019b), among others, we identify several key characteristics of UFDs that influence their dynamics during flood events:

1. The bounding box dimensions (L_x, L_y, L_z, Fig. 2A-D), which tightly contain a UFD, with L_x denoting the longest horizontal length, L_y the shortest horizontal length, and L_z the vertical height (floor-normal).
2. The total mass (M) of the UFD, which can be reciprocally defined using the UFD's bulk density (ρ_b):

$$\rho_b = \frac{M}{V} \tag{1}$$

where $V = L_x L_y L_z$ is the enclosed volume of the UFD bounding box.

3. The submerged volume (V'), which is defined as the volume contributing to buoyancy when submerged up to a water depth h. This is inherently smaller than V and is formulated as a fraction thereof (see Fig. 2D and E):

$$f_V(h) = \frac{V'}{L_x L_y h} \tag{2}$$

This ratio closely resembles porosity, which is a concept previously explored in stability models of cars (Bocanegra et al., 2020). A value of $f_V \approx 1$ suggests a fully water-tight cubic volume occupying the entirety of the volume defined by $L_x L_y h$.

4. The flow-exposed area of the bounding box, given by $A = L_x h$. For two-wheelers like scooters and bikes, which are assumed to lie on their sides (Fig. 2B), this assumption is based on the expectation that during the initial stages of flooding, two-wheelers may often topple, settling into a more stable, horizontal position.
5. The UFD effective drag area, which is the actual side area contributing to drag and is only a fraction (f_A) of the flow-exposed bounding box area (Fig. 2D and E):

$$f_A(h) = \frac{A'}{L_x h} \tag{3}$$

Here, an f_A value close to 1 implies that the UFD effectively obstructs most of the water flowing through A, while an f_A close to 0 suggests high porosity, permitting free flow of water.

6. The drag coefficient C_D, which is a dimensionless factor that quantifies how hydrodynamic the flow-exposed shape of the UFD is, and affects the fluid's drag force exerted on the effective area A'.
7. The ground clearance z_c, which is the vertical distance from the floor to the lower chassis in vehicles. Both f_A and f_V may dramatically change when water depth exceeds this clearance height.
8. The friction coefficient μ, which quantifies the ratio of frictional to normal forces between two contacting surfaces.

To address the complexity of these parameters for UFDs, we compile a comprehensive inventory, presented and detailed in Appendix A, for over 100 typified UFDs. This inventory utilizes data from online catalogues for dimensions and mass. For clearance height, an image-based manual identification method is employed. We also adopt an image-

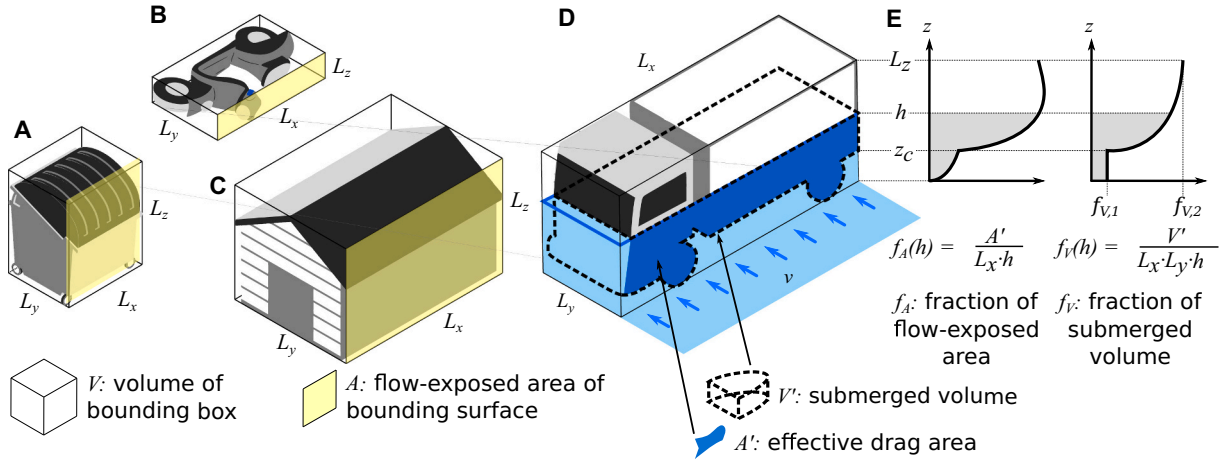

Fig. 2. Definition of the bounding box, with dimensions L_x, L_y and L_z, over an UFD of types (A) UFD-F1 (urban fixture), (B) UFD-V1 (two-wheeler), (C) UFD-F2 (household equipment) and (D) UFD-V5 (large heavy vehicle). Definition of the bounding box's total volume V ($= L_x L_y L_z$) and submerged volume V' ($= f_V L_x L_y h$), its bounding box flood-prone area A ($= L_x h$) and submerged area exposed to the flow A' ($= f_A L_x h$), and its area fraction (f_A) and volume fraction (f_V).

based routine to estimate the effective drag area (A'). This routine, applied to publicly available side images of UFDs (sources detailed in Supplementary Material), employs a binarization technique to extract the silhouette of the UFD. The fraction f_A is then calculated as the ratio between this silhouette and the flow-exposed area, under the assumption that the UFD is submerged to a specified water depth (Appendix A). For parameters like drag coefficient and submerged volume fraction, we either rely on empirically-derived values from existing literature or make simplifying geometric assumptions. For UFDs of heterogeneous composition, our estimates of physical parameters are based on reasonable assumptions such as a range of densities and expected sizes (full details and justification are included in Appendix A).

3. Mechanistic model

3.1. Limit states of stability

Aligned with previous studies (Keller and Mitsch, 1992; Smith et al., 2019b; Martínez-Gomariz et al., 2020), we establish a framework that considers the balance among four forces, drag (S_y) versus friction (R_y), buoyancy (S_z) versus weight (R_z), and two moments –toppling load (S_{yz}) versus toppling resistance (R_{yz}), as illustrated in Fig. 3 for a garbage bin, on the previously commonly identified UFDs. These correspond to three different limit states of stability. These states are associated to the types of load (S) and resistance (R), as specified in Fig. 3B: i) flotation ($S_z \geq R_z$, buoyant force exceeding weight), ii) sliding ($S_y \geq R_y$, drag force exceeding the UFD-floor friction) and iii) toppling ($S_{yz} \geq R_{yz}$, drag/buoyancy moment exceeding friction/weight moment).

3.2. Flotation

When buoyancy forces surpass the weight of an UFD, the object starts floating. For this failure mode, the destabilizing load (S_z) can be estimated as the buoyancy given by the Archimedes' principle, with ρ_w being the water density and g the gravity acceleration:

$$S_z = \rho_w g f_V (h L_x L_y) \tag{4}$$

The counteracting force or resisting component in the flotation limit state is the weight (mass $M = \rho_b L_x L_y L_z$, times gravity g):

$$R_z = \rho_b L_x L_y L_z g \tag{5}$$

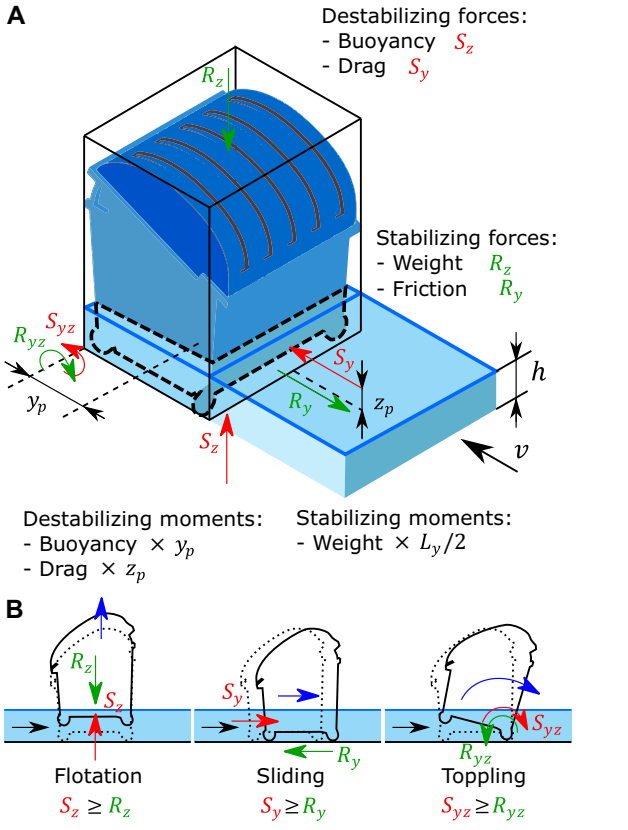

Fig. 3. Definition of (A) stabilizing and destabilizing forces and moments, and (B) limit states for the three destabilization modes.

3.3. Sliding

Sliding occurs when the drag force, acting in the y-direction, destabilizes the UFD. This load can be estimated considering the UFD effective drag area ($A' = f_A L_x h$) and the drag coefficient (C_D):

$$S_y = \frac{1}{2} \rho_w C_D f_A L_x h v^2 \tag{6}$$

The resisting component in this limit state is given by the contact friction between the UFD and the floor, and can be expressed through

the friction coefficient (μ) as:

$$R_y = \mu(R_z - S_z) \tag{7}$$

which implies that, when the normal component cancels ($R_z \rightarrow S_z$), the horizontal also cancels ($R_y \rightarrow 0$).

3.4. Toppling

Toppling may occur when the sum of destabilizing moments around an axis is larger than the sum of stabilizing moments opposing them. Taking the downstream rim of an UFD in the direction x as overturning point (Fig. 3B) allows the estimation of moments:

$$S_{yz} = S_y z_p + S_z y_p \tag{8}$$

with z_p and y_p as the lever arms at which forces S_y and S_z are applied, respectively (Fig. 3A). These lever arms depend on the distribution of pressures over the wet surface. We make a justifiable approximation by considering:

$$y_p \approx L_y/2 \tag{9}$$

and:

$$z_p \approx \begin{cases} h/2 & \text{if } h \le z_c \\ z_c + (h - z_c)/2 & \text{if } h > z_c \end{cases} \tag{10}$$

with the z_p definition acknowledging that most of the flow impacts the UFD over the level z_c, once it is submerged over the clearance height ($h > z_c$).

The toppling resistance will be given by:

$$R_{yz} = R_z L_y/2 \tag{11}$$

3.5. Limitations

The proposed mechanistic model ignores the destabilizing effect of wind or the water mass that rain can contribute, which both may be more important for small UFDs (for instance, plastics). It also ignores the effect of adhesive forces, which can be relevant for very small particles. No lift forces are considered, which are usually smaller than the drag, according to previous studies on vehicles' stability (Arrighi et al., 2015). Besides, the flow is always assumed to impact the UFD on the largest face exposed to the flow, and any interference of the flow with other UFDs is ignored, for the sake of simplicity. This is a common hypothesis in literature (Martínez-Gomariz et al., 2018; Bocanegra et al., 2020) but does not consider, for instance, that UFDs may remain in the recirculation region downstream of another UFD, or that the flow can be channelled more intensely towards them.

4. Probabilistic framework

4.1. General remarks

Utilizing the classification scheme outlined in Table 1, we categorize the properties of UFDs into three main groups: i) Vehicles (UFD-V), ii) Furniture (UFD-F), and iii) Heterogeneous UFD (UFD-H). We also incorporate all the subgroups presented in Table 1. This categorization is useful because it allows us to define tailored ranges of realistic values for all parameters used in the mechanistic model discussed in Section 3.

To identify realistic parameters for the UFDs, serving as inputs for the mechanistic model detailed in Section 3, we conduct a comprehensive examination. This examination draws upon various sources, as for instance official commercial catalogues contingent on the specific model of the typified UFDs under investigation. The survey of key properties – covering those identified in Section 2– is further elaborated in Appendix A and Supplementary Material, where all sources are included. For heterogeneous UFDs, we base our parametrization on a comprehensive literature review, complemented by justified boundaries.

In the following, we explain how we leverage this key properties' inventory for UFDs and define functional relationships and probabilistic density functions (Section 4.2 and Appendix A), which are key elements of the Monte Carlo analysis here conducted to capture the diversity inherent to each category of UFDs. The ultimate goal is to generate random, yet realistic, samples from a UFD subcategory for the purpose of performing Monte Carlo analyses of their stability, as demonstrated through the mechanistic model in Section 3. The method used includes direct sampling and this complete approach is illustrated in Fig. 4.

4.2. Structural relationships for UFDs' key variables and their variability

Each UFD, whether it be a light-weight vehicle, a trash bin, or another object, exhibits distinct characteristics, a variability that our model aims to capture. Certain characteristics, such as dimensions L_x and L_y in vehicles, often scale together –these are identified as structural relationships. These co-dependencies across multiple variables need to be considered, to ensure that, when we generate a synthetic UFD to study its stability, we are generating a realistic UFD.

In contrast, other UFD properties might exhibit randomness within defined limits and are categorized as randomistic. For such properties, we utilize Probability Density Functions (PDFs). The choice of a PDF for each variable is based on an empirical evaluation of the Cumulative Density Function, typically supplemented by physical reasoning. For example, if a characteristic must be strictly positive, a uniform distribution ($\mathscr{U}$) or a triangular distribution ($\mathscr{T}$) is favored over a Normal distribution ($\mathscr{N}$), which carries a non-zero probability of producing negative values. Either structural or randomistic, the characteristics of each UFD subcategory can be explained through the following equation:

$$y(x) = \Upsilon(x) + y' \tag{12}$$

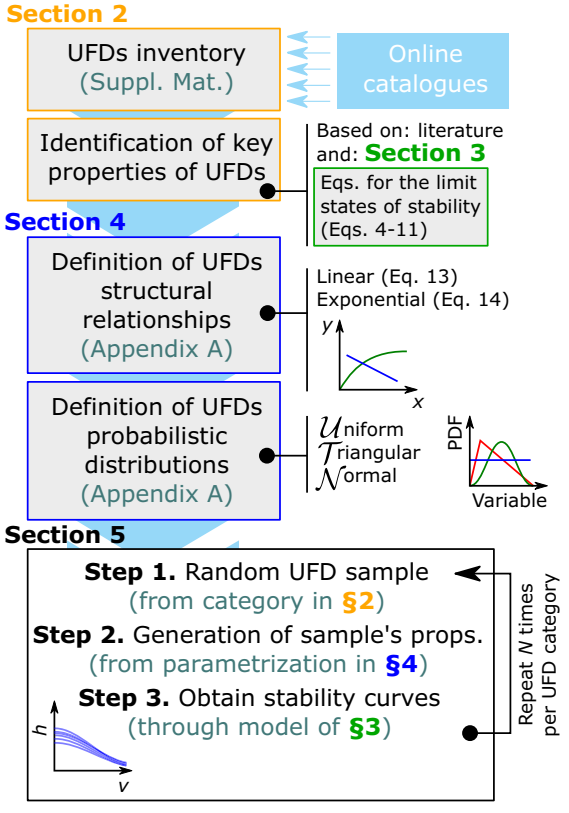

Fig. 4. Monte Carlo approach to the estimation of stability curves for different UFDs.

$\Upsilon(x)$ is a function that portrays the trend –or structural relationship– of y relative to x, while y' denotes a stochastic component that introduces additional variability into y. The functional form of $\Upsilon(x)$ is flexible, but we primarily investigate two relationships –linear and saturation curve– besides a null function:

$$\Upsilon = ax + b \tag{13}$$

$$\Upsilon = a(1 - exp(bx)) \tag{14}$$

The parameters a and b are optimized through error minimization algorithms to best fit the observed UFD data, as described in Appendix A. For certain co-dependencies, Eq. (14) offers a superior fit. For example, within all vehicles subcategories (UFD-V), an increase in L_x is accompanied by an increase in L_y, but only asymptotically up to 2.50 m, as constrained by regulations such as the European Union Council Directive 96/53/EC.

When no correlation is observed among pairs of variables, $\Upsilon(x) \equiv 0$ and only the randomistic component (y') in Eq. (12) defines an UFD characteristic (y). This is the dominant situation in UFD-H, and incorporates further variability (uncertainty) into the stability curves. For y', we consider three potential PDFs: $\mathscr{U}$, $\mathscr{T}$, or $\mathscr{N}$. A comprehensive review of the functional relationships for $\Upsilon(x)$ and the PDFs for y' across all UFD subcategories is provided in Appendix A. All relevant data and analysis codes are available in the Supplementary Material.

4.3. Monte Carlo analysis

A Monte Carlo analysis is performed to probabilistically estimate the stability curves for different UFD categories, as outlined in Table 1. This analysis is building upon the mechanistic model of Section 3 (Fig. 3) and the input parametrization defined across Section 4 and Appendix A. The procedure for the analysis is conducted for each UFD subcategory and follows the protocol here described (Fig. 4):

1. We generate 1000 different samples from a given UFD subcategory (e.g., UFD-F2), based on structural and stochastic characteristics of each group derived in Section 4.2, thereby simulating a realistic range of physical properties.
2. Stability limit state equations –for flotation, sliding, and toppling– are solved for each synthetic UFD generated.
3. For each synthetic UFD, the minimum depth h required to initiate motion at a given velocity v is identified by considering all three instability modes and is designated as the value for the stability curve.
4. Results are visualized and data is stored by UFD group in the Supplementary Material.

4.4. Limitations

The proposed probabilistic approach directly draws samples from PDFs for the key physical properties of UFDs, which at the same time define secondary physical properties through the structural relationships. A limitation of this methodology is that we assume simple PDF functions for those key physical properties as well as for the structural relationships between parameters. This is reasonable based on the available data, and provided that we have partitioned UFDs into groups (Table 1) with similar characteristics. Another limitation is that the empirical data defining those PDFs is based on catalogues available online, primarily, whereas some UFDs found in urban areas may be old enough to not be currently online.

5. Results

5.1. Application and verification of the mechanistic framework

In this section, we utilize various case studies from literature (Table 2) to evaluate the accuracy and applicability of the mechanistic model proposed in Section 3. We focus the verification study on cars (UFD-V2, light-weight vehicles Table 1), owing to the wealth of available research data. Fig. 5 presents both the experimental data from literature and the predicted limit states of our mechanistic model (Section 3).

Some parameters (M, L_x, L_y, L_z, z_c), necessary for the application of the model (Eqs. (4) to (11)), are directly incorporated from the original case studies. In all instances, we consider the friction coefficient (μ) as 0.3, in line with reporting from laboratory experiments (see study of Smith et al., 2019b). For the evaluation of f_A at each depth, we use the data-driven polynomial approximation specified for UFD-V2 in Appendix A (Eq. (A3), excluding the stochastic term f_A'). Unspecified parameters such as $f_{V,2}$ and, occasionally, C_D are calibrated iteratively. Given that C_D impacts stability at high flow velocities, while $f_{V,2}$ is influential at low velocities, these parameters can be calibrated independently. We recognize that the drag coefficient (C_D) varies among the considered case studies. This variation is reasonable and can be justified on geometrical differences in shapes of car models.

Inspection of Fig. 5 reveals that the stability limit state curves generated by our model, in conjunction with physical properties, are physically consistent and describe the laboratory data in good detail. At near-zero velocities, flotation becomes the governing instability mode. For non-zero velocities, buoyancy lowers the threshold for sliding and toppling by reducing the effective normal force ($R_y - S_y$, see Eqs. (7) and (8)). The stability curves exhibit a notable flattening as water levels drop below the clearance height (z_c), which corresponds to a diminishing effect of f_A and f_V. In all our verification cases, toppling proves to be a less likely failure mode than either sliding or flotation, occurring at relatively lower water depths.

5.2. Probabilistic assessment of stability curves

In this subsection, we extend the application of the mechanistic model to encompass all UFD groups, deploying the previously outlined Monte Carlo simulation approach (see Fig. 4) that follows the inherent variability of UFDs. For clarity, Figs. 6F, 7C and Fig. 8F incorporate flow conditions based on uniform flow estimations, which are based on the Manning formula (Chow, 1959). This enables the estimation of pairs of h-v for a given slope and roughness coefficient. These highlighted regions within the plots intersect the stability curves, thereby identifying the conditions under which UFDs' mobility is likely to be initiated. For that, we consider a wide array of slopes and surface roughness, ranging from smooth cement to gravel bed, with corresponding Manning numbers $n = 0.011$ to 0.025. These are representative of reasonable surfaces and slopes found in urban setups. The highest value of the Manning coefficient ($n = 0.025$) is also representative of short grass.

Our probabilistic analysis of vehicles' stability reveals several critical insights (Fig. 6):

- Two-wheelers (UFD-V1) are generally less stable than other vehicle types. However, some V1 vehicles possess higher bulk density than water (due to small internal volumes, metal construction and no cabin). This results in a threshold velocity below which they remain unconditionally stable; i.e., sinking regardless of the flow depth.
- Cars (UFD-V2) exhibit stability conditions very similar to those seen in the verification cases, with the dispersion of the data aligning with the variability observed in the verification cases. This reaffirms that this type of UFD is well represented in the literature.
- Vans (UFD-V3), caravans and RVs (UFD-V4) demonstrate a behavior comparable to UFD-V2, although caravans exhibit a considerably

Table 2
Key characteristics of the UFD-V2 models used for verification. The f_A used is that parameterized in Appendix A for UFD-V2, Eq. (A3), with stochastic term $f_{A'} = 0$. f_{V1} corresponds to the submerged volume contribution of the wheels, assumed constant, and f_{V2} corresponds to the above-clearance contribution. Values with (*) correspond to best fit (calibrated), which is only conducted for missing data.

Car	M (kg)	L_x (m)	L_y (m)	L_z (m)	z_c (m)	C_D (−)	f_{V1} (−)	f_{V2} (−)	μ (−)	Exp. scale	Source
Yaris	1045	4.30	1.69	1.46	0.16	1.38	0.05	0.32*	0.30	1:1	Smith et al. (2019b)
Festiva	790	3.62	1.61	1.46	0.22	1.38	0.05	0.32*	0.30	1:1	Smith et al. (2019b)
Golf	1261	4.26	1.80	1.45	0.21	1.70*	0.05	0.42*	0.30	1:1	Kramer et al. (2016)
Accord	1615	4.95	1.85	1.48	0.12	0.75*	0.05	0.58*	0.30	1:14/1:24	Xia et al. (2014)
Patrol	2478	4.97	1.84	1.94	0.50	1.38	0.05	0.50*	0.30	1:1	Smith et al. (2019b)
Q7	2345	5.09	1.98	1.74	0.20	0.85*	0.05	0.50*	0.30	1:14/1:24	Xia et al. (2014)

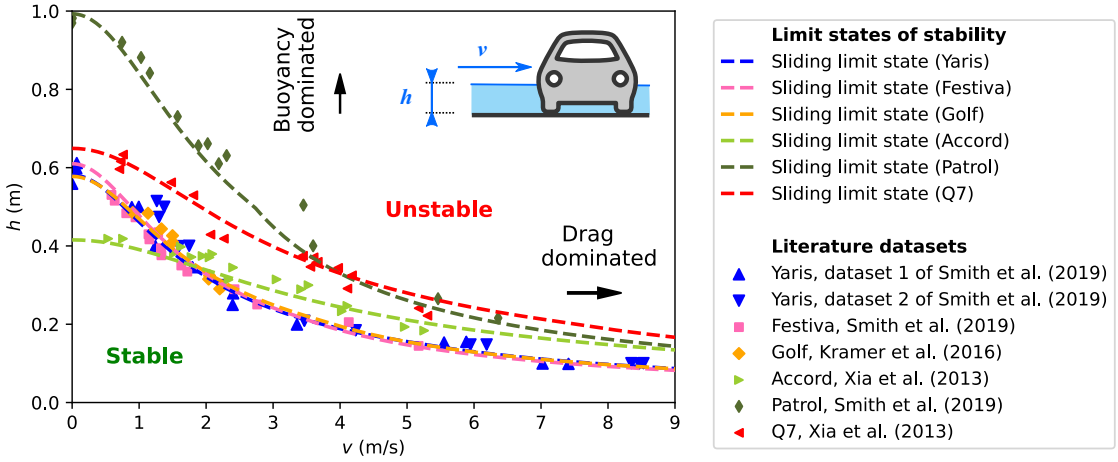

Fig. 5. Stability curves obtained with the mechanistic model (Section 3) for specific car models tested in laboratory in literature (Xia et al., 2014; Kramer et al., 2016; Smith et al., 2019b).

narrower distribution of stability curves. This is because, with increasing size, bulk density tends to reduce for habitable vehicles. Therefore, both vans and caravans tend to be less stable than cars on flatter slopes when flotation becomes the dominant mode of failure. This early onset of mobility, coupled with their larger volumes, increases flood hazard due to a higher potential for infrastructure clogging and damage. Given that these larger vehicles are commonly observed in flood events, mitigating flood hazards would require additional focus on UFD-V3 and UFD-V4.

– Heavy vehicles (UFD-V5), owing to their massive scale, exhibit substantially higher stability. However, this category exhibits a wider dispersion due to the considerable range of properties; for instance, L_x ranges from 6 to 18 m. Our findings suggest that these vehicles could contribute to flood hazards under flood situations with depths exceeding 1 m, particularly when also exposed to high velocities ($v > 2$ m/s). UFD-V5, with masses one to two orders of magnitude greater than other UFD-Vs, may substantially amplify potential infrastructure damage due to impacts (Zhang et al., 2018; Jalayer et al., 2018), in addition to the also increased flood-infrastructure clogging hazard.

When considering furniture (UFD-F), it is evident that both UFD-F1 and UFD-F2 are highly movable. Urban fixtures (UFD-F1) become unstable at approximate depths of 25 cm, which is consistent with previous studies (Martínez-Gomariz et al., 2020), while household equipment (UFD-F2) exhibits instability at depths significantly below 10 cm. This signals an earlier onset of transport as compared to vehicles. Nonetheless, UFD-F2 are commonly installed within private properties, potentially attenuating the direct impact of flooding. The disclosed early mobility of UFD-F suggests that the role of furniture in urban floods might have been consistently underestimated.

For heterogeneous debris and drifters (UFD-H), our analysis (Fig. 8) indicates that stability characteristics are closely related to the material density. Plastic debris is the least stable, with the vast majority of items becoming mobilized at water depths of below a few centimeters. This is followed closely by other litter, which shows a very similar behavior. Wood remains considerably more stable up to flood depths of 10 cm for low velocities (< 1 m/s). Velocities and depths observed are consistent with the wood stability study of Braudrick and Grant (2000). The most stable types within the UFD-H category are construction materials and metal, which require exceptionally large velocities for the inception of mobility – of at least 3 to 5 m/s – typically becoming dislodged only after impacts from other UFDs (such as trucks or cars) with infrastructure or when located near construction sites adjacent to streets.

6. Discussion

6.1. Sequential mobilization of UFDs

As a synthesis of the results presented in Figs. 6, 7 and 8, we sequence the mobilization of UFDs due to an idealised flood hydrograph (large enough to mobilise all groups of UFDs), which is presented in Fig. 9. In a real flood risk analysis, information obtained from a 2D hydrodynamic model ($h - v$) can be used to assess which UFDs become unstable, when their potential locations within urban setups are known. For a low-slope configuration, Fig. 9 illustrates such sequence (with potentially metal and construction debris not being transported), whereas for a high slope, vans, caravans and RVs (UFD-V3-V4) would be expected to move after cars (UFD-V2). The sequence of Fig. 9 allows, based on visual identification of selected UFDs in future floods imagery, to infer which other groups of UFDs have already been mobilized. Likewise, observation of mobilized urban furniture, for instance, can allow reconstruction of local flow depths (likewise Moy de Vitry et al., 2019) and velocities at selected locations, while images in social media can also be dated (Valero et al., 2021); therefore, allowing a space and time reconstruction of the flood.

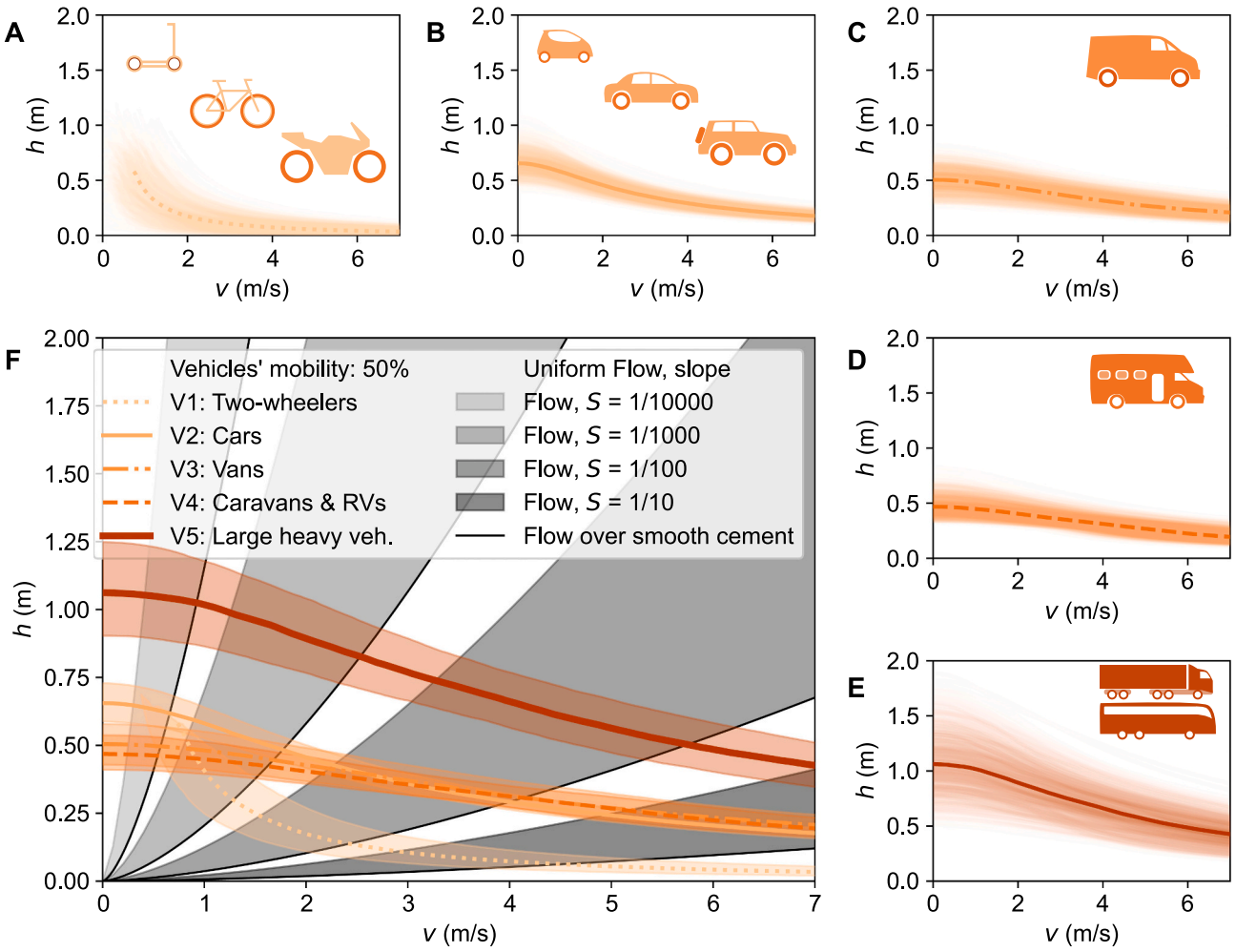

Fig. 6. Stability curves for vehicles: A Two-wheelers (UFD-V1), B Cars (UFD-V2), C vans (UFD-V3), D caravans & RVs (UFD-V4), E heavy vehicles (UFD-V5). F Vehicles stability curves intersection with uniform flow over different urban surfaces (from smooth cement to excavated gravel, Chow, 1959) at different slopes.

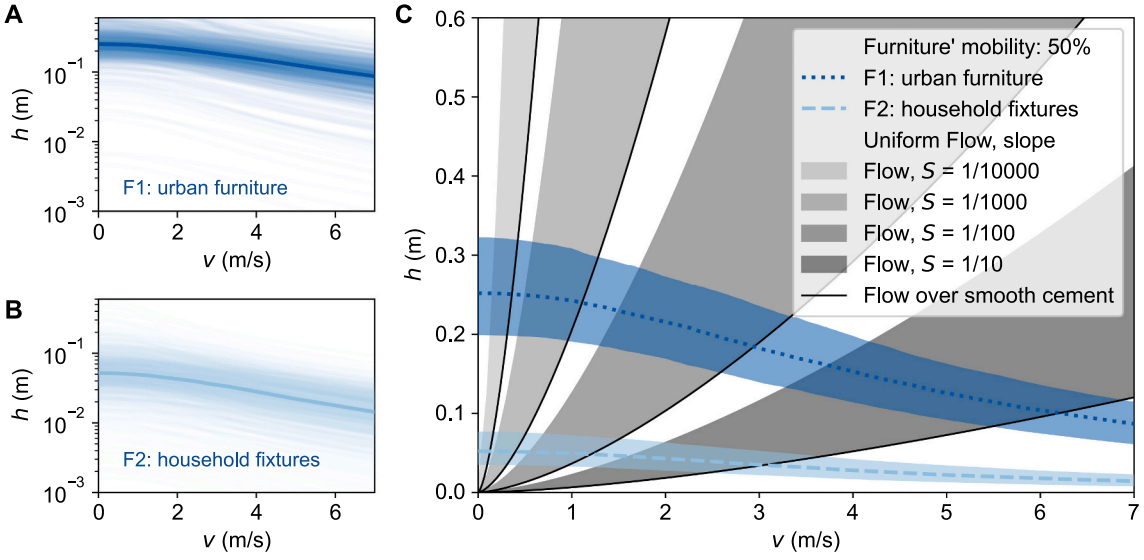

Fig. 7. Stability curves for furniture: A urban furniture (UFD-F1), B private furniture (UFD-F2). C Furniture stability curves intersection with uniform flow over different urban surfaces (from smooth cement to excavated gravel, Chow, 1959) at different slopes.

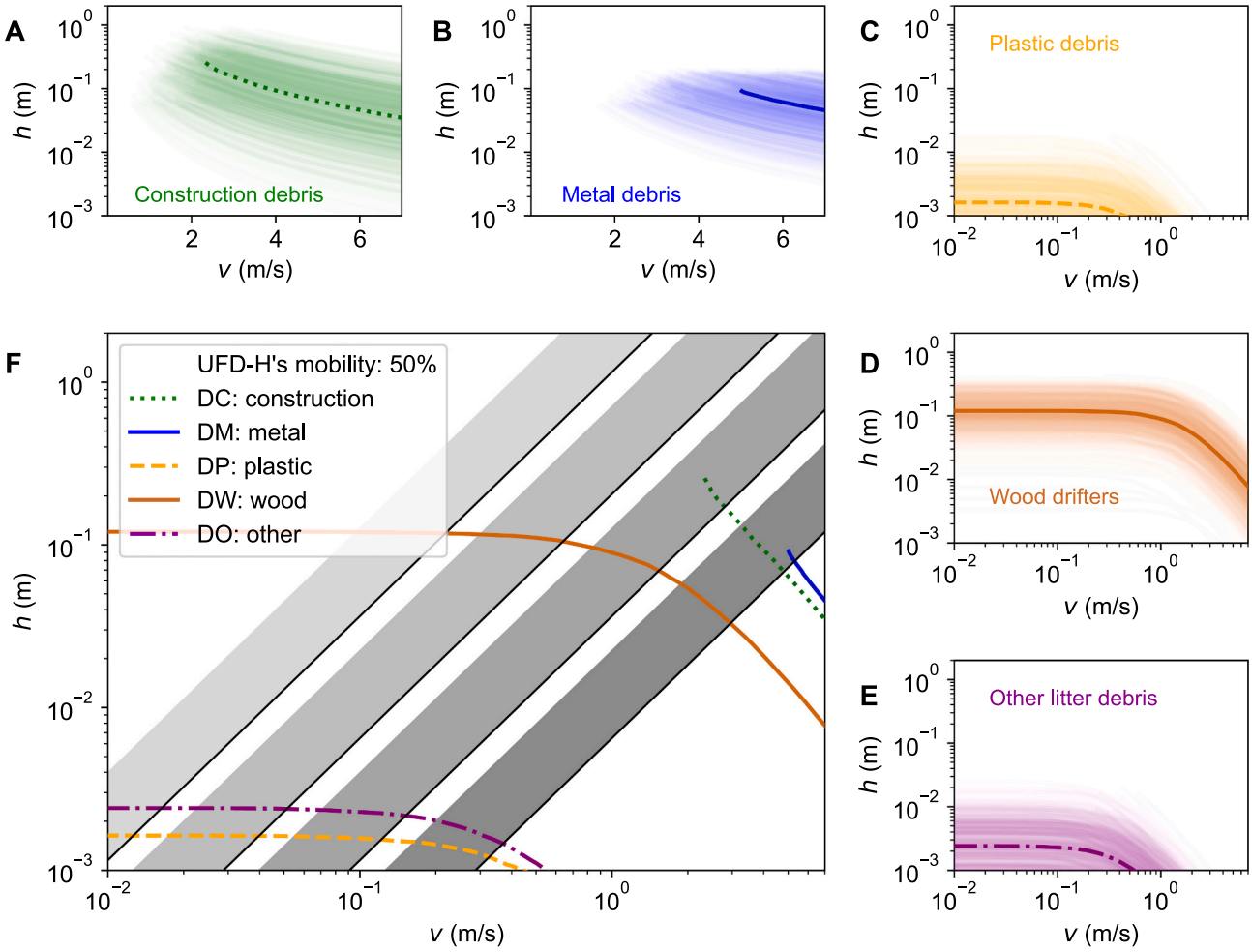

Fig. 8. Stability curves for UFD-H: A construction debris (UFD-DC), B metal debris (UFD-DM), C plastic debris (UFD-DP), D wood (UFD-DW), E other debris (UFD-DO). F Heterogeneous UFD curves intersection with uniform flows over different urban surfaces at different slopes (same as in Fig. 6, from smooth cement to excavated gravel, Chow, 1959) at different slopes.

6.2. Flood risk implications

The diversity of debris mobilized by floods poses a challenge to flood risk management, especially in urban areas. The landscape in flood-prone areas should be carefully designed, not only considering cars, but the wider variety of potentially movable –flood hazard– material (Table 1 and Fig. 9). This is especially important in regions with higher flood risk, where new developments are often allowed with additional mitigation or resilience measures (European Commission, 2021). In such spaces, especial effort should be put to avoid creating sources of UFDs or by enabling extra mooring mechanisms.

Some regulations contemplate hazard induced by cars (UFD-V2) within the flood risk analysis (Shand et al., 2011), others even raise caravans as potentially unstable in flood waters (Australian Institute for Disaster Resilience, 2017), and some suggest a threshold at about 25 cm for increased hazard due to debris transport (European Commission, 2021). However, to the knowledge of the authors, none explicitly covers the specific thresholds of instability of the wide range of debris here analysed and, although regulations for cars have been found to be conservative in the context of car-induced hazards (Shand et al., 2011; Smith et al., 2019b), other UFDs are more movable or of potentially larger hazard. Another point raised in the flood-risk literature (Bocanegra et al., 2020) is the very limited range of cars analysed in previous hydrodynamics research. In this context, our study is especially important, because it tackles both previous gaps (in regulations and scientific literature) by addressing a wide range of potentially movable material, as well as tackling their full probability density functions for their characteristics, providing specific combinations of flow velocities and depths that trigger their movement.

While identifying and avoiding sources of UFDs is essential in floodplains, further insights can be gained by looking further downstream. Our study provides a reference point for the inception of movement, but their transport can be especially complex, especially for finite-sized bodies (Valero et al., 2022; Delhez et al., 2023; Lofty et al., 2024). If velocities are known in a 2D grid, obtained through 2D flood modelling, these can be used to obtain streamlines starting at the identified UFD sources. This allows the identification of the potential transport routes. When these streamlines encounter contractions smaller than the maximum size of the UFD mobilized (Table A1 for UFD-V and UFD-F, and Table A3 for UFD-H), a substantial and sudden backwater flooding can be triggered because of the clogging of infrastructure (Kramer et al., 2015; Schalko et al., 2018). These flood bottlenecks, defined by the combination of large debris and small cross-section, should be prevented by all means.

6.3. Environmental implications

From a pollution prevention perspective, we show that relatively low flows can mobilise most of the heterogeneous UFDs, except for that generated from construction material and metal, which furthermore requires damage to infrastructure (Jalayer et al., 2018; Zhang et al., 2018) to be available for transport. Even when available for transport, a

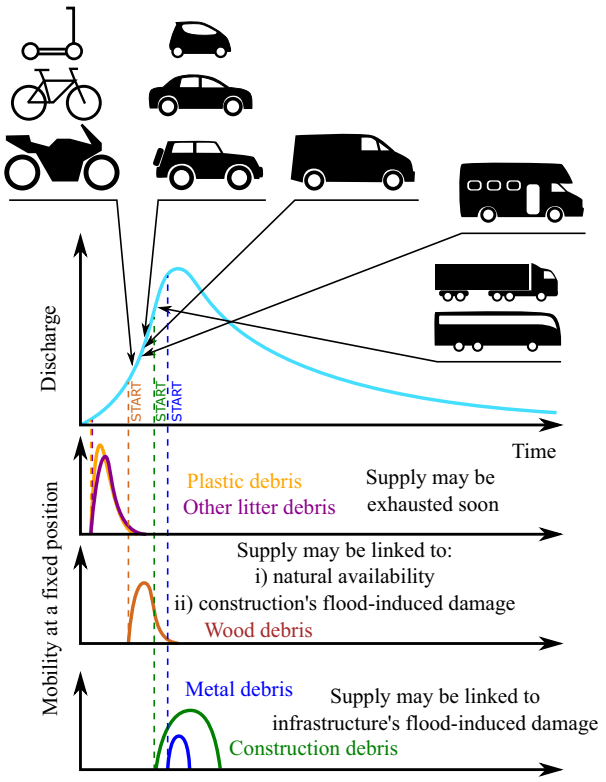

Fig. 9. Sequential UFD mobility at varying flood hydrograph stages, based on probabilistic onset calculations of Figs. 6, 7 and 8.

swift reduction in flow conditions can cause this debris to settle rapidly, potentially resulting in limited conveyance distance.

Most of the litter (UFD-DP and UFD-DO), however, can be expected to be transported with depths below 5 mm, which means that newly flooded areas will readily have all their litter transported, becoming part of the flood. This low requirement for mobilization also implies that direct runoff to rivers can cause an uncontrolled pollution source even for low flows, becoming vectors of distal pollution. This may become more evident in regions with constrained or limited waste management services and infrastructure, where litter supply may be overwhelmingly larger during the washout (Moulds et al., 2022; Akuoko et al., 2023; Oludele et al., 2023).

Overflown floodplains can also become sinks of litter during receding flows, particularly when the flood returns to the river banks. These sinks can again act as sources during future floods, potentially enabling an intermittent transport across seasons or even years. For very large floods, litter should find sufficient transport capacity, and their transport only be impeded when interacting with structures or vegetation (Schreyers et al., 2021). This aligns with previous hydrological observations on litter pollution (van Emmerik et al., 2019; Van Emmerik et al., 2019; van Emmerik et al., 2022).

7. Conclusions

This investigation addresses the estimation of the inception of movement of different urban loose objects, here referred as UFDs. These have characteristics (length scales and mass, for instance) spanning several orders of magnitude, which leads to a large difference in the combination of velocities and depths that trigger their movement. The derived stability curves, available in the Supplemental Material, can be integrated into 2D flood models. Coupled with source/supply estimations, these curves can enable, for the first time, the prediction of UFDs' travel patterns during flooding events. This is a key step towards the identification of high-risk zones for clogging and backwater effects, thereby potentially enhancing urban flood risk mitigation strategies.

Our findings show that –against prior expectations– vans, caravans and RVs (UFD-V3–4) can be more mobile than other UFDs such as lightweight vehicles, while also having a larger mass and size and therefore an increased hazard. Caravans and RVs are often parked near rivers and streams, which may enhance their flood exposure. When planning such spaces, flood risk aspects should also be considered. A key aspect revealed by this study is the relevance of the placement of urban furniture and their mooring conditions. Solely relying on their weight is shown to be insufficient, given that furniture (UFD-F) is very often more mobile than vehicles (UFD-V). Another aspect to consider is that plastic (UFD-DP) and other litter (UFD-DO) can be mobilized under frequent flow conditions, with runoff of just a few millimetres, 10–100 times smaller flow depths than for the mobilization of wood (UFD-DW). This highlights how important is to reduce availability to avoid direct transport into the environment in areas close to rivers and streams. Other debris such as metal or construction may remain completely stable regardless of the flow depth, for flow velocities below 2–4 m/s, suggesting that special care should be put in protecting them from floods in high-slope areas.

A relevant limitation of our study is that we consider UFDs isolated, where flow effects do not consider interaction with other UFDs, nor we consider impacts of other movable UFDs with the stable ones. For very small UFDs, such as plastics, other forces not considered (such as adherence) could contribute to further stabilize them. Future studies may also need to address the downstream transport; i.e., dynamics of the UFDs after the incipient motion. Based on the results presented in this study, we argue that actions can already be taken in urbanised areas, via urban planning for instance, to reduce the impacts of flooding, both in terms of damage to property and life endangering as well as in terms of environmental impacts. Where UFDs are expected to be placed in flood-sensitive areas, additional efforts should be put to avoid their associated hazards.

CRediT authorship contribution statement

Daniel Valero: Writing – review & editing, Writing – original draft, Visualization, Validation, Software, Methodology, Investigation, Formal analysis, Conceptualization. **Arnau Bayón:** Writing – review & editing, Writing – original draft, Visualization, Validation, Software, Methodology, Investigation, Data curation, Conceptualization. **Mário J. Franca:** Writing – review & editing, Writing – original draft, Resources, Methodology, Conceptualization.

Declaration of competing interest

The authors declare that they have no conflict of interest.

Data availability

The codes producing the stability curves (as well as all the stability curves) are available under: https://doi.org/10.5281/zenodo.10880333. This also includes the physical properties of UFDs and their sources. The codes (mechanistic model and Monte Carlo analysis) are implemented in Python 3, using built-in functions of Numpy (Harris et al., 2020).

Acknowledgments

The authors are grateful for the discussions they had with Dr. Isabella Schalko regarding wood properties and mobilization. This research was partially supported by the Erasmus+ STA Program (European Union), the research projects CIGE/2022/7 and CIAEST/2021/56 (Generalitat Valenciana, Spain), and the research projects PACAP-2022 and PAID-06-22 (Universitat Politècnica de València, Spain). Fig. 1.A was reproduced with AFP' permission. Fig. 1.B was reproduced with AP's permission.

Fig. 1.C was reproduced with Getty Images' permission.

Appendix A. Supplementary data

Supplementary data to this article can be found online at https://doi.org/10.1016/j.scitotenv.2024.171568.

References

AFP, 2023. Flash floods kill at least 14 in Turkish quake zone. In: Dawn – Agence France Presse. https://www.dawn.com/news/1742343 (accessed: 2023-09-05).

Akuoko, I.S.G., Vandenberg, J., Falman, J.C., Otsuka, K., Lau, G.K., Skrobe, M., An, S., Faustman, E.M., Ota, Y., 2023. Rethinking plastic realities in Ghana: a call for a well-being approach to understanding human-plastics entanglements for more equitable plastics governance. Mar. Policy 158 (105 856).

Argyroudis, S.A., Mitoulis, S.A., Winter, M.G., Kaynia, A.M., 2019. Fragility of transport assets exposed to multiple hazards: state-of-the-art review toward infrastructural resilience. Reliab. Eng. Syst. Saf. 191 (106 567).

Arrighi, C., 2021. A global scale analysis of river flood risk of UNESCO world heritage sites. Front. Water 12. https://doi.org/10.3389/frwa.2021.764459.

Arrighi, C., Alcèrreca-Huerta, J., Oumeraci, H., Castelli, F., 2015. Drag and lift contribution to the incipient motion of partly submerged flooded vehicles. J. Fluids Struct. 57, 170–184.

Arrighi, C., Oumeraci, H., Castelli, F., 2017. Hydrodynamics of pedestrians' instability in floodwaters. Hydrol. Earth Syst. Sci. 21, 515–531.

Arrighi, C., Pregnolato, M., Dawson, R., Castelli, F., 2019. Preparedness against mobility disruption by floods. Sci. Total Environ. 654, 1010–1022.

Australian Institute for Disaster Resilience, 2017. Managing the Floodplain: A Guide to Best Practice in Flood Risk Management in Australia, Online. https://knowledge.aidr.org.au/media/3521/adr-handbook-7.pdf.

Bates, P.D., Savage, J., Wing, O., Quinn, N., Sampson, C., Neal, J., Smith, A., 2023. A climate-conditioned catastrophe risk model for UK flooding. Nat. Hazards Earth Syst. Sci. 23, 891–908.

Bayón, A., Valero, D., Franca, M.J., 2023. Urban Flood Drifters (UFDs): Identification, Classification and Characterisation, (Preprint).

Bocanegra, R.A., Vallés-Morán, F.J., Francés, F., 2020. Review and analysis of vehicle stability models during floods and proposal for future improvements. J. Flood Risk Manag. 13, e12 551.

Braudrick, C.A., Grant, G.E., 2000. When do logs move in rivers? Water Resour. Res. 36, 571–583.

Browder, G., Nunez Sanchez, A., Jongman, B., Engle, N., Van Beek, E., Castera Errea, M., and Hodgson, S. n.d.: An EPIC Response: Innovative Governance for Flood and Drought Risk Management, World Bank, Washington, D.C.

Chow, V., 1959. T.: Open-Channel Hydraulics. The Blackburn Press.

Clement, V., Rigaud, K.K., de Sherbinin, A., Jones, B., Adamo, S., Schewe, J., Sadiq, N., Shabahat, E., 2021. Groundswell Part 2: Acting on Internal Climate Migration. World Bank. https://openknowledge.worldbank.org/handle/10986/36248.

Davidson, S., MacKenzie, L., Eaton, B., 2015. Large wood transport and jam formation in a series of flume experiments. Water Resour. Res. 51 (10 065–10 077).

Delhez, C., Riviére, N., Erpicum, S., Pirotton, M., Archambeau, P., Arnst, M., Bierens, J., Dewals, B., 2023. Drift of a drowning victim in rivers: conceptualization and global sensitivity analysis under idealized flow conditions. Water Resour. Res. 59, e2022WR034 358.

Dewals, B., Erpicum, S., Pirotton, M., Archambeau, P., 2021. July 2021 extreme floods in the Belgian part of the Meuse basin. Hydrolink 4.

van Emmerik, T., Strady, E., Kieu-Le, T.-C., Nguyen, L., Gratiot, N., 2019. Seasonality of riverine macroplastic transport. Sci. Rep. 9, 1–9.

van Emmerik, T., Frings, R., Schreyers, L., Hauk, R., de Lange, S., Mellink, Y., 2022. River plastic during floods: Amplified mobilization, limited river-scale dispersion, preprint at. https://www.researchsquare.com/article/rs-1909246/v1.

European Commission, 2021. Current Practice in Flood Risk Management in the European Union, Tech. Rep., European Commission, Directorate-General for Environment, Luxembourg. https://doi.org/10.2779/235272.

European Environment Agency, 2022. Economic losses from climate-related extremes in Europe. https://www.eea.europa.eu/ims/economic-losses-from-climate-related (accessed: 2022-06-10).

Getty Images, 2012. China doubles Beijing flood death toll, CNN – Getty Images. https://edition.cnn.com/2012/07/26/world/asia/china-beijing-flood/index.html (accessed: 2023-09-05).

Goral, K.D., Guler, H.G., Larsen, B.E., Carstensen, S., Christensen, E.D., Kerpen, N.B., Schlurmann, T., Fuhrman, D.R., 2023. Shields Diagram and the Incipient Motion of Microplastic Particles. Environmental Science & Technology.

Hammond, M.J., Chen, A.S., Djordjević, S., Butler, D., Mark, O., 2015. Urban flood impact assessment: a state-of-the-art review. Urban Water J. 12, 14–29.

Harris, C.R., Millman, K.J., Van Der Walt, S.J., Gommers, R., Virtanen, P., Cournapeau, D., Wieser, E., Taylor, J., Berg, S., Smith, N.J., et al., 2020. Array programming with NumPy. Nature 585, 357–362.

Hickey, J.T., Salas, J.D., 1995. Environmental effects of extreme floods. In: Hydrometeorology, Impacts, and Management of Extreme Floods, pp. 13–17.

Jalayer, F., Aronica, G.T., Recupero, A., Carozza, S., Manfredi, G., 2018. Debris flow damage incurred to buildings: an in situ back analysis. J. Flood Risk Manag. 11, S646–S662.

Jonkman, S., Vrijling, J., 2008. Loss of life due to floods. J. Flood Risk Manag. 1, 43–56. https://doi.org/10.1111/j.1753-318X.2008.00006.x.

Kahn, M.E., 2005. The death toll from natural disasters: the role of income, geography, and institutions. Rev. Econ. Stat. 87, 271–284.

Keller, R., Mitsch, B., 1992. Stability of cars and children in flooded streets. In: Proceedings of International Symposium on Urban Stormwater Management, Sydney, Australia.

Kramer, M., Peirson, W., French, R., Smith, G., 2015. A physical model study of culvert blockage by large urban debris. Australas. J. Water Res. 19, 127–133.

Kramer, M., Terheiden, K., Wieprecht, S., 2016. Safety criteria for the trafficability of inundated roads in urban floodings. Int. J. Disast. Risk Reduct. 17, 77–84. https://doi.org/10.1016/j.ijdrr.2016.04.003.

Lindersson, S., Raffetti, E., Rusca, M., Brandimarte, L., Márd, J., Di Baldassarre, G., 2023. The wider the gap between rich and poor the higher the flood mortality. Nat. Sustain. 1–11.

Lofty, J., Valero, D., Wilson, C.A., Franca, M.J., Ouro, P., 2023. Microplastic and natural sediment in bed load saltation: material does not dictate the fate. Water Res. 243, 120329.

Lofty, J., Valero, D., Moreno-Rodenas, A., Belay, B.S., Wilson, C., Ouro, P., Franca, M.J., 2024. On the vertical structure of non-buoyant plastics in turbulent transport. Water Res. 254, 121306.

Ludwig, P., Ehmele, F., Franca, M.J., Mohr, S., Caldas-Alvarez, A., Daniell, J.E., Ehret, U., Feldmann, H., Hundhausen, M., Knippertz, P., et al., 2023. A multi-disciplinary analysis of the exceptional flood event of July 2021 in central Europe. Part 2: historical context and relation to climate change. Nat. Haz. Earth Syst. Sci. Discuss. 23, 1287–1311. https://doi.org/10.5194/nhess-23-1287-2023.

Martínez-Gomariz, E., Gómez, M., Russo, B., 2016. Experimental study of the stability of pedestrians exposed to urban pluvial flooding. Nat. Hazards 82, 1259–1278.

Martínez-Gomariz, E., Gómez, M., Russo, B., Djordjevi'c, S., 2018. Stability criteria for flooded vehicles: a state-of-the-art review. J. Flood Risk Manag. 11, S817–S826.

Martínez-Gomariz, E., Russo, B., Gómez, M., Plumed, A., 2020. An approach to the modelling of stability of waste containers during urban flooding. J. Flood Risk Manag. 13, e12 558.

Mellink, Y.A., van Emmerik, T., Mani, T., 2023. Wind- and Rain-driven Macroplastic Mobilization and Transport on Land. https://doi.org/10.21203/rs.3.rs-3452848/v1.

Mignot, E., Li, X., Dewals, B., 2019. Experimental modelling of urban flooding: a review. J. Hydrol. 568, 334–342. https://doi.org/10.1016/j.jhydrol.2018.11.001.

Milanesi, L., Pilotti, M., 2020. A conceptual model of vehicles stability in flood flows. J. Hydraul. Res. 58, 701–708. https://doi.org/10.1080/00221686.2019.1647887.

Mohr, S., Ehret, U., Kunz, M., Ludwig, P., Caldas-Alvarez, A., Daniell, J.E., Ehmele, F., Feldmann, H., Franca, M.J., Gattke, C., et al., 2023. A multi-disciplinary analysis of the exceptional flood event of July 2021 in central Europe–Part 1: event description and analysis. Nat. Hazards Earth Syst. Sci. 23, 525–551.

Moulds, S., Chan, A.C., Tetteh, J.D., Bixby, H., Owusu, G., Agyei-Mensah, S., Ezzati, M., Buytaert, W., Templeton, M.R., 2022. Sachet water in Ghana: a spatiotemporal analysis of the recent upward trend in consumption and its relationship with changing household characteristics, 2010–2017. PLoS One 17, e0265 167.

Moy de Vitry, M., Kramer, S., Wegner, J.D., Leitão, J.P., 2019. Scalable flood level trend monitoring with surveillance cameras using a deep convolutional neural network. Hydrol. Earth Syst. Sci. 23, 4621–4634.

O'Donnell, E.C., Thorne, C., 2020. R.: drivers of future urban flood risk. Phil. Trans. R. Soc. A 378, 20190 216.

Oludele, S.M., Samuel, A., Omosat, O.K., 2023. Unveiling Environmental Governance and Political Economy Dynamics in Rural Plastic Pollution Management: A Case Study of Ogun State. Nigeria, Reality of Politics, pp. 74–113.

Pregnolato, M., Ford, A., Wilkinson, S.M., Dawson, R.J., 2017. The impact of flooding on road transport: a depth-disruption function. Transp. Res. Part D: Transp. Environ. 55, 67–81.

Roberson, J., 2008. Iowa river ebbs, but levees in Illinois, Des Moines fail, Chron – Associated Press. https://www.chron.com/news/nation-world/article/Iowa-river-ebbs-but-levees-in-Illinois-Des-1771585.php (accessed: 2023-09-05).

Sanders, B.F., Schubert, J.E., Kahl, D.T., Mach, K.J., Brady, D., AghaKouchak, A., Forman, F., Matthew, R.A., Ulibarri, N., Davis, S.J., 2023. Large and inequitable flood risks in Los Angeles, California. Nat. Sustain. 6, 47–57.

Schalko, I., Schmocker, L., Weitbrecht, V., Boes, R.M., 2018. Backwater rise due to large wood accumulations. J. Hydraul. Eng. 144, 04018 056.

Schreyers, L., Van Emmerik, T., Nguyen, T.L., Castrop, E., Phung, N.-A., Kieu-Le, T.-C., Strady, E., Biermann, L., van Der Ploeg, M., 2021. Plastic plants: the role of water hyacinths in plastic transport in tropical rivers. Front. Environ. Sci. 9, 177.

Shah, S.M.H., Mustaffa, Z., Martinez-Gomariz, E., Kim, D.K., Yusof, K.W., 2021. Criterion of vehicle instability in floodwaters: past, present and future. Int. J. River Basin Manag. 19, 1–23. https://doi.org/10.1080/15715124.2019.1566240.

Shand, T., Cox, R., Blacka, M., Smith, G., 2011. Australian Rainfall and Runoff Project 10: Appropriate Safety Criteria for Vehicles, Tech. Rep.; Eng.

Smith, A., Bates, P.D., Wing, O., Sampson, C., Quinn, N., Neal, J., 2019a. New estimates of flood exposure in developing countries using high-resolution population data. Nat. Commun. 10, 1814.

Smith, G.P., Modra, B.D., Felder, S., 2019b. Full-scale testing of stability curves for vehicles in flood waters. J. Flood Risk Manag. 12, e12527 https://doi.org/10.1111/jfr3.12527.

United Nations, 2020. How climate change is making record-breaking floods the new normal. https://www.unep.org/news-and-stories/story/how-climate-change-making-record-breaking-floods-new-normal (accessed: 2022-06-12).

United Nations, 2023. The United Nations World Water Development Report 2023: Partnerships and Cooperation for Water. https://www.unesco.org/reports/wwdr/2023/en/download (accessed: 2023-05-31).

Valero, D., Schalko, I., Friedrich, H., Abad, J.D., Bung, D.B., Donchyts, G., Felder, S., Ferreira, R.M., Hohermuth, B., Kramer, M., et al., 2021. Pathways towards Democratization of Hydro-Environment Observations and Data, IAHR White Paper Series.

Valero, D., Belay, B.S., Moreno-Rodenas, A., Kramer, M., Franca, M.J., 2022. The key role of surface tension in the transport and quantification of plastic pollution in rivers. Water Res. 226, 119078.

Van Emmerik, T., Tramoy, R., Van Calcar, C., Alligant, S., Treilles, R., Tassin, B., Gasperi, J., 2019. Seine plastic debris transport tenfolded during increased river discharge. Front. Mar. Sci. 6, 642.

Waldschläger, K., Schüttrumpf, H., 2019. Erosion behavior of different microplastic particles in comparison to natural sediments. Environ. Sci. Technol. 53, 13 219–13 227.

Wing, O.E., Lehman, W., Bates, P.D., Sampson, C.C., Quinn, N., Smith, A.M., Neal, J.C., Porter, J.R., Kousky, C., 2022. Inequitable patterns of US flood risk in the Anthropocene. Nat. Clim. Chang. 12, 156–162.

Winsemius, H.C., Jongman, B., Veldkamp, T.I., Hallegatte, S., Bangalore, M., Ward, P.J., 2018. Disaster risk, climate change, and poverty: assessing the global exposure of poor people to floods and droughts. Environ. Dev. Econ. 23, 328–348.

World Economic Forum, 2022. The Global Risks Report 2022. https://www.weforum.org/reports/global-risks-report-2022/ (accessed: 2022-10-25).

Xia, J., Falconer, R.A., Xiao, X., Wang, Y., 2014. Criterion of vehicle stability in floodwaters based on theoretical and experimental studies. Nat. Hazards 70, 1619–1630.

Zevenbergen, C., Gersonius, B., Radhakrishan, M., 2020. Flood resilience. Phil. Trans. R. Soc. A 378, 20190 212.

Zhang, S., Zhang, L., Li, X., Xu, Q., 2018. Physical vulnerability models for assessing building damage by debris flows. Eng. Geol. 247, 145–158.